

## CONTACTLESS METHOD FOR RESISTANCE MEASUREMENT OF ULTRA-THIN PRINTED AND CONDUCTIVE LINES

**Krzysztof Szybiński**

Wrocław University of Science and Technology, Chair of Electronic and Photonic Metrology, ul. B. Prusa 53/55, 50-317 Wrocław, Poland (✉ [krzysztof.szybinski@pwr.edu.pl](mailto:krzysztof.szybinski@pwr.edu.pl), +48 663 033 991)

### Abstract

In this paper the problem of resistance measurement of ultrathin conductive lines on dielectric substrates dedicated for printing electronic industry is discussed. The measured line is transformed in a non-invasive way into a resonance circuit. By using a magnetic coupling between the source line and the tested line, the resistance measurement can be performed non-invasively, *i.e.* without a mechanical contact. The proposed contactless resistance measurement method is based on the resonance quality factor estimation and it is an example of the inverse problem in metrology.

Keywords: inkjet printing electronics, resistance measurements, micrometer conducting lines, contactless method, resonance circuits.

© 2020 Polish Academy of Sciences. All rights reserved

### 1. Introduction

In growing inkjet printing electronic industry many quality tests of printing lines are conducted [1]. To define the quality of manufactured printed lines many tests are conducted, such as resistance measurements, which have to meet certain norms depending on their technological application. To measure the inkjet printing lines resistance specialist probe stations which consist of advanced microscopes, micromanipulators and precise measurement needle probes are used [2]. Figure 1 illustrates an example of a resistance measurement setup.

Measurements with such a probe station require a well-qualified operator. The current conductive lines printing techniques enable the production of micron-scale lines [3]. Development of this technology is related to the Flat Panel Displays industry advancement. It turns out now that the manufacturing of display matrices is very sensitive to various mechanical as well as environmental factors. As a result, a lot of displays do not pass the final quality test [4]. The inkjet printing electronics technology makes it possible to repair damaged display matrices at the production stage and lower the manufacturing costs, reducing both the number of potential electronic waste and the environmental pollution [5].



Fig. 1. MPS150 probe station by Form Factor company [2].

To meet the industrial requirements the research centers which develop the inkjet printing lines techniques need to constantly test their new technologies. As mentioned earlier, the line resistance is one of the fundamental parameters to be evaluated during the production process. To measure the resistance of a line which is several microns wide it is necessary to use very thin probes to puncture into opposite ends of a measured line. Figure 2 shows the needle probe connection process using the four point resistance measurement method.

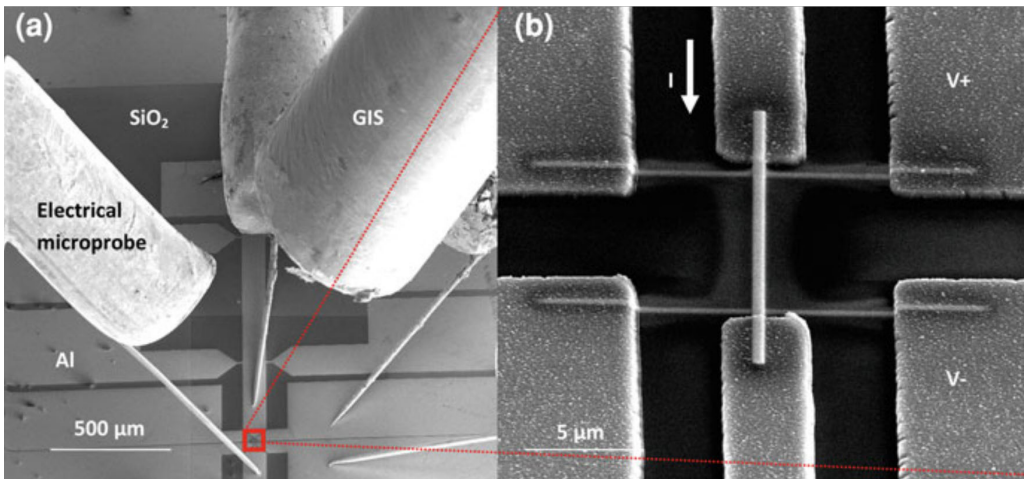


Fig. 2. (a) SEM image of experimental configuration for 4-wire electrical measurements. (b) SEM image of one deposited line (magnification) [7]

(Reprinted by kind permission of Dr Amalio Fernandez-Pacheco).

Probe manipulation requires a lot of skill from the operator. Furthermore founding the measured line under the microscope and then placing the probes carefully with adequate force into the line is time-consuming. The probes used for such measurements are disposable and expensive. In addition, such micro-scale measurements are accompanied by a constriction resistance which reveals itself especially at small contact area and probe distortion during measurements [6].

The constriction resistance problem can be reduced by a four-point Kelvin resistance measurement method, however, it leads to an increase in the complexity of the measurement system by an additional pair of probes [7]. What more, either the line or the substrate can be scratched when the operator accidentally moves the probe during the clamping process. This can happen as a result of a high thrust point action on a tested line. What more, careless operation by the operator, who can move the probe during its clamping, may scratch the line or substrate.

Development of the printing process is preceded by a validation which relies on various electrical (*e.g.*, resistance measurements) as well as non-electrical tests (*e.g.*, adhesion analysis [8]). As the samples produced this way are expensive, reducing the possibility of damage is very desirable at the early stage of this process. In this manuscript a non-invasive method for printing line resistance measurements is proposed and discussed in which the risk of careless damage is reduced. For this reason, in the proposed approach I delimit the specialized probe station usage in printing line testing process to the case of lines which meet the method requirements.

This paper presents a contactless resistance measurement method in which the mechanism of magnetic coupling between the tested line and the source line is used. The tested sample is transformed into a resonant circuit in a non-invasive way by placing the conductive surface beneath the dielectric substrate which creates a flat capacitor whose electrodes are tested line and a conductive surface beneath the substrate, respectively. The created capacitor is characterized by series inductance and measured resistance which are the line parameters. The resistance measurement is based on amplitude-frequency characteristic mapping of new resonant circuit by measuring current changes during frequency sweeping. The capacitance and inductance of a tested sample are calculated on the basis of the line and substrate parameters. This measurement process is an example of an inverse problem in metrology [9].

## 2. Line and substrate parameters determination

Special test paths are developed in research centers which deal with printing electronic technology to assess the quality of printing methods. Tested lines are characterized by certain geometric parameters such as width, height and length. From electrical point of view the line is characterized by some resistance and inductance. These properties are related to geometric and material parameters including the resistivity. Figure 3 shows a cross-sectional view of the measured line on the dielectric substrate. The conductive lines printing process uses conductive inks, based on *e.g.*, silver [10]. To achieve a conductive crystalline structure, the lines are subjected to a sintering process [11]. Furthermore, the conductive ink after the sintering process cannot reach the resistivity like its bulk equivalent [12], hence a resistivity of the material cannot be

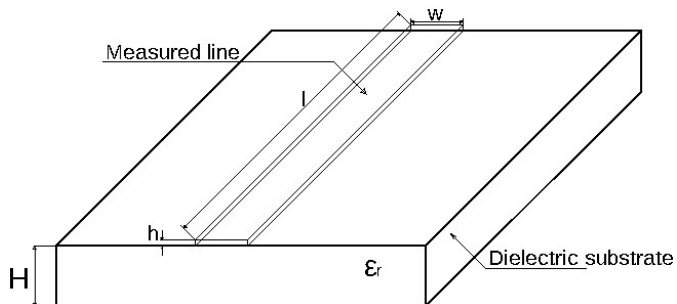


Fig. 3. The cross-section of the inkjet printed conductive line – the examined sample.

defined accurately. Also, during the sintering process the tested line can be damaged. Due to the above facts the line resistance must be measured rather than only calculated.

The proposed method requires a definition of inductance of the examined line. The inductance of a line segment depends on its geometry [13]. All geometric parameters can be measured with no physical contact with the line under the test by using, e.g., the image processing methods embedded in modern microscopes [14] or by using a scanning electron microscope (SEM) [15]. Having the dimensions of the examined line it is possible to define its inductance using the following formula [16]:

$$L [\mu\text{H}] = 2 \cdot 10^{-3} l \left[ \ln \left( \frac{2l}{w+h} \right) + 0.5 + 0.2235 \left( \frac{w+h}{l} \right) \right], \quad (1)$$

where  $w$  [cm] is the line width,  $l$  [cm] is the line length and the  $h$  [mm] – is the line thickness.

Assuming the following line dimensions for the further considerations  $l = 20$  cm,  $w = 20$   $\mu\text{m}$ ,  $h = 100$  nm and using the formula (1) the considered line inductance is about 416 nH. The formula (1) is also used to calculate e.g. microstrip lines inductance and can be applied a wide range of frequencies, due the fact that the straight line has no parasitic capacitance and magnetic core losses.

To determine the measurement error of the inductance the general propagation of uncertainty formula is used:

$$\Delta L = \sqrt{\left( \frac{\partial L}{\partial l} \cdot \Delta l \right)^2 + \left( \frac{\partial L}{\partial w} \cdot \Delta w \right)^2 + \left( \frac{\partial L}{\partial h} \cdot \Delta h \right)^2}, \quad (2)$$

where  $\Delta l = \pm 10^{-3}$  [cm],  $\Delta w = \pm 10^{-4}$  [cm],  $\Delta h = \pm 2 \cdot 10^{-5}$  [mm], are the measurement errors which are related to the length, width and thickness of examined line measurement respectively. The errors above are related to the quality of the optical instruments of the modern microscopes and the image processing methods embedded in them. The image processing methods capabilities in the modern microscopes were discussed in [17] in details.

In order to calculate inductance measurement error all of the partial derivatives values were calculated (3) to (5).

$$\frac{\partial L}{\partial l} = 3 \cdot 10^{-3} + 2 \cdot 10^{-3} \ln \left( \frac{2l}{w+h} \right) \cong 0.0227, \quad (3)$$

$$\frac{\partial L}{\partial w} = \frac{4.47x \cdot 10^{-4} - 2y \cdot 10^{-3} + 4.47z \cdot 10^{-4}}{x+z} \cong -19.047, \quad (4)$$

$$\frac{\partial L}{\partial h} = \frac{4.47x \cdot 10^{-4} - 2y \cdot 10^{-3} + 4.47z \cdot 10^{-4}}{x+z} \cong -19.047. \quad (5)$$

After the calculation it turns out that the  $\partial L/\partial w$  and  $\partial L/\partial h$  are equal. However, the final formula (2) cannot be simplified due to this fact. This is caused by different measurement errors and different units in the inductance formula for each derivative. Subsequently by substituting all of the errors and partial derivatives values into formula (3) the resultant inductance measurement error will be 3.8 nH. Hence the final inductance value can be described as  $L = (416 \pm 3.8)$  nH.

The proposed method requires the sample under test must to be transformed into a flat capacitor. This can be achieved by placing the conductive surface, e.g. a copper plate, beneath the dielectric substrate in a non-invasive way. This transformation is illustrated in Fig. 4. Assuming

that the substrate is made of 100  $\mu\text{m}$  thick silicon, the capacitance, of a parallel plate capacitor from Fig. 4 is:

$$C = \frac{\varepsilon_0 \cdot \varepsilon_r \cdot S}{H} = 4.14 \text{ pF}, \quad (6)$$

where  $S [\text{m}^2] = w [\text{m}] \cdot l [\text{m}]$ ,  $H$  is the substrate thickness,  $\varepsilon_0$  is the permittivity of free space equal to  $8.854 \cdot 10^{-12} [\text{F/m}]$  and  $\varepsilon_r = 11.68$  is the relative permittivity of a silicon surface. According to (6), the sample capacity is about 4.14 pF.

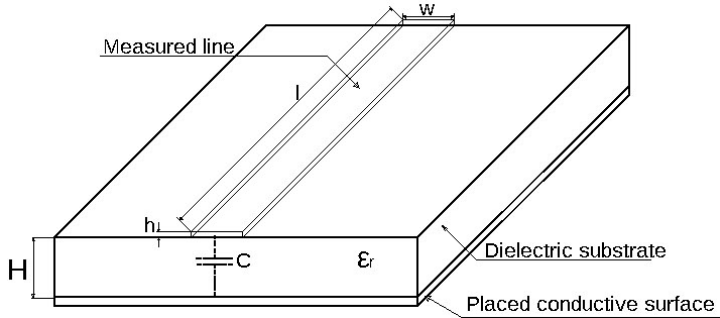


Fig. 4. Flat capacitor sample. A thin conductive path under test is placed on the top of a silica substrate with an electrode film from the bottom. The dashed line represents the equivalent element formed in the circuit.

In accurate capacitance estimation the relation between substrate material permittivity and frequency at which the measurement takes place should be taken into consideration as this may cause capacitance change at some frequency ranges. However, the materials, such as silicon are characterized by good stability of permittivity over the frequency range that is used in the examined case. A noticeable change occurs when the frequency reaches dozens of gigahertz [18].

In order to determine the capacitance measurement error the general propagation of uncertainty formula is used:

$$\Delta C = \sqrt{\left(\frac{\partial C}{\partial H} \cdot \Delta H\right)^2 + \left(\frac{\partial C}{\partial w} \cdot \Delta w\right)^2 + \left(\frac{\partial C}{\partial l} \cdot \Delta l\right)^2 + \left(\frac{\partial C}{\partial \varepsilon} \cdot \Delta \varepsilon\right)^2}, \quad (7)$$

where  $\Delta l = \pm 10^{-5} [\text{m}]$ ,  $\Delta w = \pm 10^{-6} [\text{m}]$  are the measurement errors which are related to the length and width of the examined line measurement respectively.  $\Delta H$ , is the substrate thickness measurement error equal to  $\pm 10^{-6} [\text{m}]$  and  $\Delta \varepsilon = \pm 1.034 \cdot 10^{-12} [\text{F/m}]$ , is the silicon dielectric permittivity uncertainty estimation.

In order to calculate capacitance measurement error all of the partial derivatives values were obtained (8) to (11).

$$\frac{\partial C}{\partial H} = \frac{\varepsilon \cdot w \cdot l}{H^2} \cong 4.14 \cdot 10^{-8}, \quad (8)$$

$$\frac{\partial C}{\partial w} = \frac{\varepsilon \cdot l}{H} \cong 2.07 \cdot 10^{-7}, \quad (9)$$

$$\frac{\partial C}{\partial l} = \frac{\varepsilon \cdot w}{H} \cong 2.07 \cdot 10^{-11}, \quad (10)$$

$$\frac{\partial C}{\partial \varepsilon} = \frac{l \cdot w}{H} \cong 4 \cdot 10^{-2}. \quad (11)$$

Having all the partial derivatives, the final value of the measurement error, according to formula (7) is 0.22 pF. Hence the final capacitance value can be described as  $C = (4.14 \pm 0.22)$  pF.

Based on calculated capacity and inductance, the input data for proposed method was obtained. In the next chapter the operation principle of contactless resistance measurement will be described. The calculated inductance and capacitance measurement errors were used subsequently as the tolerances of components value in a Monte Carlo analysis and the resistance uncertainty propagation analysis.

### 3. Measurement method

By short-circuiting one of the ends of the tested line with the ground of the circuit from Fig. 4, a resonant circuit is formed consisting of a parallel connection of the capacitor and inductor, through the measured resistance. The idea of measurement setup is illustrated in Fig. 3. A function generator is connected to the source line ( $L_1$ ) through the impedance matching circuit which provides impedance matching between the output of a generator and the source line. One of the ends of  $L_1$  is connected to the conductive substrate which acts as the capacitor electrode in secondary circuit, via low impedance flat plate.

The measurement method is based on the magnetic coupling between the source line ( $L_1$ ) and the measured line ( $L_2$ ). Due to the fact that the resonant frequency of the tested circuit is independent of mutual inductance  $M$  and depends on the secondary circuit parameters, it can be described by the following formula:

$$f_0 = \frac{1}{2\pi\sqrt{LC}}, \tag{12}$$

where  $L$  [H] is the considered line inductance,  $C$  [F] is the capacitance between measured line and the conductive surface.

Figure 6 illustrates the equivalent circuit of the measurement setup from Fig. 5. The circuit was drawn using the Tina Ti software. The circuit from Fig. 6 is characterized by some quality factor related to its bandwidth. The quality factor depends on the measured resistance and it is described by the following formula:

$$Q = \frac{1}{R}\sqrt{\frac{L}{C}}, \tag{13}$$

where  $R$  is the resistance of measured line.

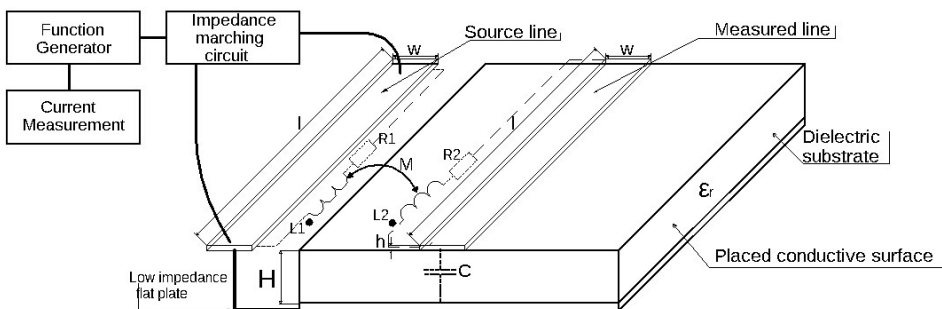


Fig. 5. Diagram of the measurement system, illustrating the idea of contactless resistance measurement by using the magnetic coupling.

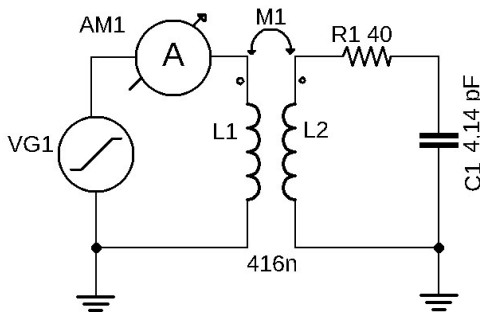


Fig. 6. Equivalent circuit of the proposed measurement system.

The quality of the resonance circuit can be also described by the resonance frequency to bandwidth ratio:

$$Q = \frac{f_0}{\Delta f}, \tag{14}$$

where  $f_0$  is the circuit resonance frequency,  $\Delta f$  is the  $-3$  dB bandwidth which is the difference between upper and lower frequencies:

$$\Delta f = f_H - f_L, \tag{15}$$

where  $f_H$  is the circuit upper frequency and  $f_L$  is the circuit lower frequency. By combining (13) with (14) and rearranging, the following formula for  $R$  may be derived:

$$R = \frac{\Delta f}{f_0} \cdot \sqrt{\frac{L}{C}}. \tag{16}$$

Apart from the inductance and capacitance, the upper, center, and lower frequency values are necessary to calculate the line resistance. Due to the fact that at the resonance frequency no current flows through the parallel circuit, it is possible to define this frequency indirectly by measuring the current in source line  $L_1$ . In practice, the measured current value will be at its lowest in resonance. The circuit center frequency value estimation comes down to finding a minimum current value.

In order to find the minimum value of the circuit current the sweeping mode of the generator should be used. The sweeping starting point is the theoretical resonance frequency value calculated in Section 2. The measured current value at the resonance frequency is the starting point to determine lower and upper circuit frequencies. This value is now the starting point to determine the lower and upper circuit frequencies. The expected amplitude-frequency characteristic of the measured circuit will be symmetric around the center frequency. Due to this fact, the measured current values at lower and upper frequencies will be 3 dB higher than the current value at the resonance frequency. The flowchart in Fig. 9 illustrates the proceeding in definition of upper, lower and center frequencies of measured circuit. By following the algorithm instructions all the necessary data for the measured line resistance estimation can be obtained.

Figure 7 shows the gain of the circuit from Fig. 6 as a function of frequency. According to Fig. 7, the resonance, upper and lower frequency values are:  $f_0 - 120.98$  MHz,  $f_L - 113.91$  MHz,  $f_H - 129.12$  MHz. The circuit bandwidth is thus:

$$\Delta f = 129.12 \text{ MHz} - 113.91 \text{ MHz} = 15.21 \text{ MHz}. \tag{17}$$

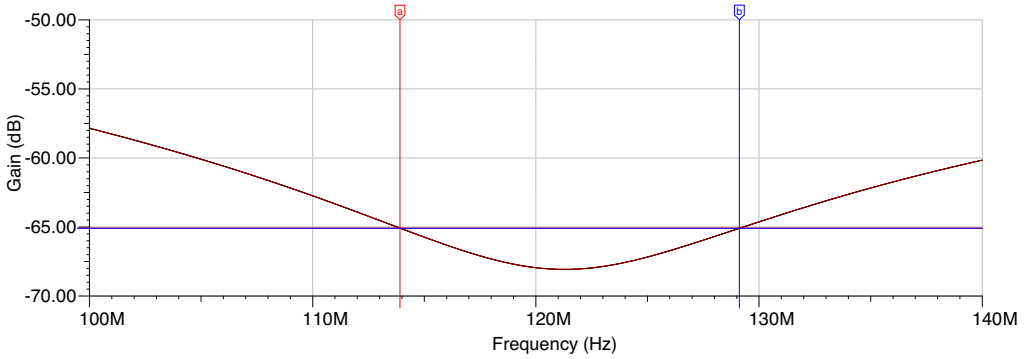


Fig. 7. Amplitude-frequency characteristics of the tested resonance circuit ( $R_1=40 \Omega$ ).

For  $R$ ,  $L$ ,  $C$  values from Fig. 6 the assumed resistance ( $R_1$ ) value on which the simulation was based is  $40 \Omega$  per  $20 \text{ cm}$  line and  $20 \mu\text{m}$  width. The printed line resistance depends on both geometric parameters as well as material parameters which are both related to the ink properties such as composition, concentration and size of nanoparticles affecting its resistivity. In [19] different line resistances can be found depending on line width and ink properties described as a unit resistance, often as  $[\Omega/\mu\text{m}]$ .

To investigate the accuracy of the proposed method  $R_1$  value must be assumed as unknown and subsequently calculated on the basis of the line inductance [ $L = (416 \pm 3.8) \text{ nH}$ ], circuit capacitance [ $C = (4.14 \pm 0.22) \text{ pF}$ ] and the frequencies obtained from the circuit simulation,  $f_0 - 120.98 \text{ MHz}$ ,  $\Delta f - 15.21 \text{ MHz}$ .

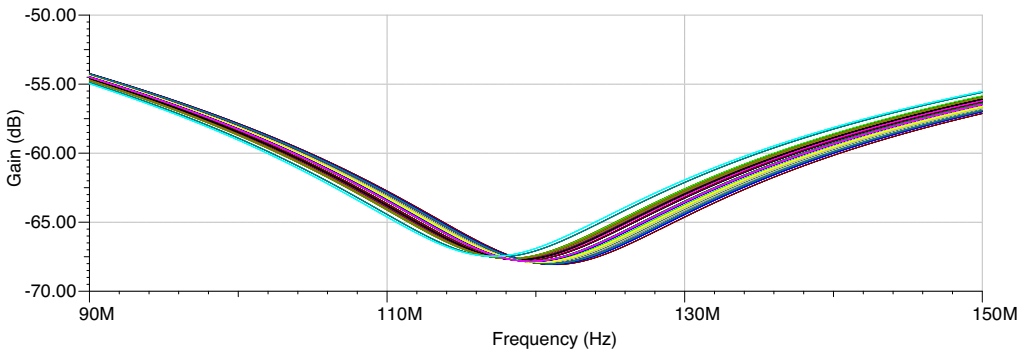


Fig. 8. Amplitude-frequency characteristics of the tested resonance circuit ( $R_1 = 40 \Omega$ ) – Monte Carlo analysis mode. Number of Monte Carlo runs ( $n = 40$ ); percent of population ( $\sigma = 95\%$ ).

By substituting the data above to (16) the estimated line resistance ( $R_{s1}$ ) is:

$$R_{s1} = \frac{15.21}{120.98} \cdot \sqrt{\frac{416}{0.00414}} \cong 39.85 \Omega, \quad (18)$$

where  $R_1$  is the real resistance value and the  $R_{s1}$  is the calculated line resistance based on the simulation results.

A Monte Carlo analysis [20, 21] was performed to determine the measurement error of the resistance  $R_{s1}$ . The following tolerances were applied to parts in the schematic in Fig. 6:  $C_1$  ( $\pm 5.2\%$ ) and  $L_2$  ( $\pm 0.91\%$ ). The circuit response was analyzed by performing an AC sweep from 90 MHz to 150 MHz. The number of Monte Carlo runs ( $n$ ) was 40 and the percent of population ( $\sigma$ ) was 95%. The distribution of components tolerances was Gaussian. Figure 8 shows the amplitude-to-frequency characteristics for the circuit form Fig. 6 performing a Monte Carlo analysis. Each curve was subjected to analysis in order to determine the resonant (characteristic) frequencies as well as the 3 dB bandwidth. To characterize deviations between predicted and observed values the root-mean-square errors of both the resonant frequency (19) and bandwidth were calculated (20).

$$\sigma_{f_0} = \sqrt{\frac{\sum_{i=1}^n (f_{0i} - \bar{f}_0)^2}{n-1}} \cong 1.3 \cdot 10^6 \text{ Hz}, \quad (19)$$

where  $\bar{f}_0$ , is the mean value of resonant frequency of all ( $n$ ) simulation results and  $f_{0i}$  is the subsequent frequency value.

$$\sigma_{\Delta f} = \sqrt{\frac{\sum_{i=1}^n (\Delta f_i - \overline{\Delta f})^2}{n-1}} \cong 8.4 \cdot 10^4 \text{ Hz}, \quad (20)$$

where  $\overline{\Delta f}$ , is the mean value of bandwidth of all ( $n$ ) simulation results and  $\Delta f_i$  is the subsequent bandwidth value. The root-mean-square errors values from (19) and (20), were subsequently used in order to calculate the resistance measurement error.

By knowing the inductance, capacitance and both frequencies errors, the measurement error of the line resistance ( $\Delta R$ ) can be estimated:

$$\Delta R = \sqrt{\left(\frac{\partial R}{\partial L} \cdot \Delta L\right)^2 + \left(\frac{\partial R}{\partial C} \cdot \Delta C\right)^2 + \left(\frac{\partial R}{\partial f_0} \cdot \sigma_{f_0}\right)^2 + \left(\frac{\partial R}{\partial \Delta f} \cdot \sigma_{\Delta f}\right)^2}, \quad (21)$$

where:  $\Delta L = 3.8 \cdot 10^{-9}$  [H],  $\Delta C = 2.15 \cdot 10^{-13}$  [F], error  $\sigma_{f_0} = 1.3 \cdot 10^6$  [Hz],  $\sigma_{\Delta f} = 8.4 \cdot 10^4$  [Hz], are the inductance, capacitance, resonant frequency and bandwidth measurements measurement errors, respectively.

In order to calculate the resistance measurement error, all the partial derivatives values were calculated (22) to (25).

$$\frac{\partial R}{\partial \Delta f} = \frac{\sqrt{L}}{f_0 \sqrt{C}} \cong 2.62 \cdot 10^{-6}, \quad (22)$$

$$\frac{\partial R}{\partial f_0} = \frac{-\Delta f \sqrt{L}}{f_0^2 \sqrt{C}} \cong 3.29 \cdot 10^{-7}, \quad (23)$$

$$\frac{\partial R}{\partial C} = \frac{-\Delta f \sqrt{L}}{2 f_0 \sqrt{C}^3} \cong -1.397 \cdot 10^4, \quad (24)$$

$$\frac{\partial R}{\partial L} = \frac{\Delta f}{2 f_0 \sqrt{L} \sqrt{C}} \cong 3.81 \cdot 10^7. \quad (25)$$

For the combination of the above partial derivatives, the line resistance measurement error following (21) is 0.7  $\Omega$ .

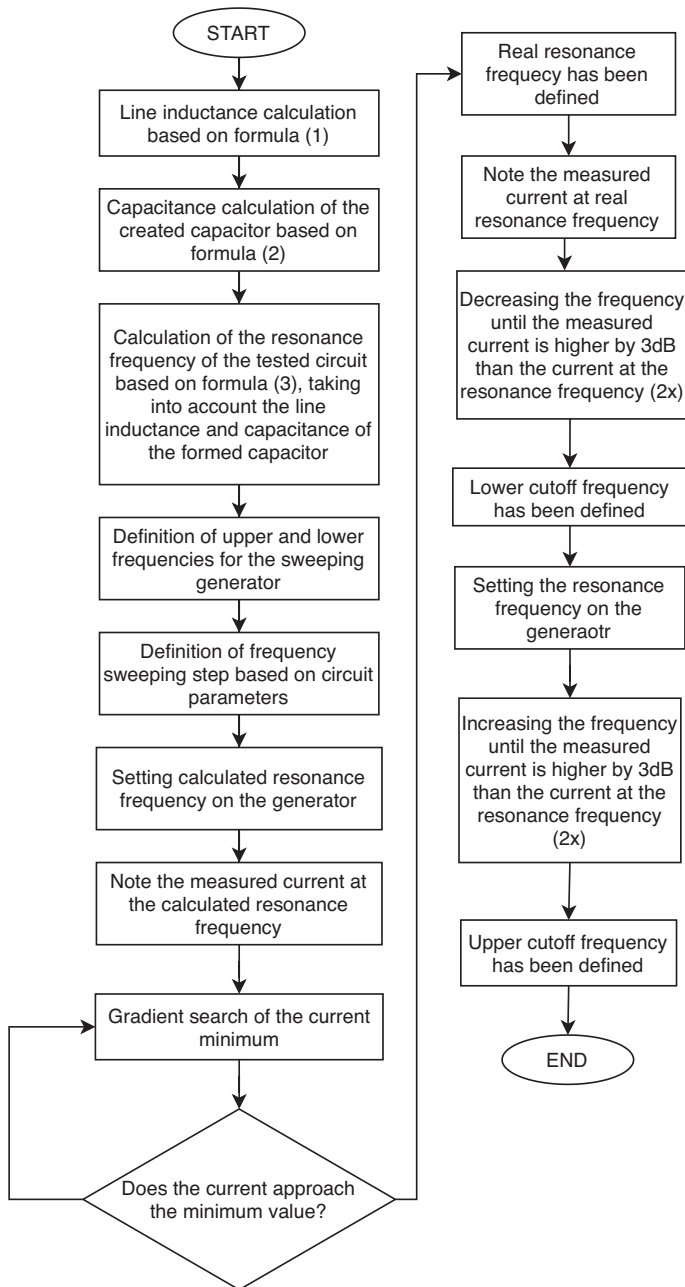


Fig. 9. The algorithm flow chart for the upper, lower and center frequencies definition in tested circuit.

#### 4. Summary

The presented contactless resistance measurement method determines the resistance of ultra-thin printed and conductive lines commonly used in flat panel display technology. The main

advantage of the proposed method is elimination of the tested line damage done during measurements. The probe measurement stations use high accuracy and resolution multimeters [22] which are characterized by the precision higher than that achieved in the proposed method. Using the commercial probe station for measuring the samples with a limited adhesion causes a risk that the manufactured line can be damaged by a high pressure caused by point action of a needle probe. The proposed method cannot replace the specialized probe stations in all of their applications. However it can be used especially during the early development stages of a printing technology where the samples manufacturing is expensive and vulnerable.

The final measurement error of the considered line resistance was evaluated at 1.75%. This error was estimated using mathematical modelling and computer simulations. In accuracy evaluation, a number of physical parameters of the equivalent electrical circuit such as inductance, capacitance, resonant frequency and bandwidth were taken into account. The resonant circuit parameters described above are determined indirectly. Hence, the line resistance error value depends on the accuracy of estimation of the resonant circuit parameters above.

The accuracy of the line inductance and capacitance estimation depends on a precise determination of the line and substrate dimensions. The estimated measurement errors for the line inductance and capacitance were 0.91% and 5.2% respectively. These error values were evaluated by using the propagation of uncertainty formula.

The numerical error value evaluation for the resonant frequency and bandwidth of the tested circuit were 1.08% and 0.55%, respectively. These error values were determined on the basis of the Monte Carlo analysis. The root-mean-square errors of both the resonant frequency and bandwidth were calculated based on the deviations between predicted and observed values. It should, however, be noted that the computer simulations do not take into account many factors that may occur in a practical application. As discussed in Section 2, it is possible to determine the geometrical dimensions of the tested line accurately and thus its inductance. On the other hand, the capacity estimations require a precise determination of the dielectric constant of the substrate as a function of frequency [23]. It is worth noting here that depending on substrate type and line dimensions the resultant resonant circuit components values will be different. For shorter lines and a substrate having lower dielectric permittivity, the resonance frequency of analyzed circuit may occur at a frequency higher by an order of magnitude. Hence the presented measurement errors values should be considered as a reference point for accuracy the proposed method. To apply the proposed method it is necessary to use both a very stable function generator [24] as well as wide frequency range current measurement system.

In consequence, the obtained resistance measurement error of the examined line, equal to 1.75% should be considered as reference accuracy of the proposed method, rather than as universal and constant error value.

The topics related to a practical application of the contactless resistance measurement method are reserved for future work. Some practical tasks such as maximization of the magnetic coupling between the source inductance and the tested line, as well as its influence on the resonance circuit frequency will be taken.

## References

- [1] Jiazhen S., Jiang J., Bao B., Wang S., He M., Zhang X. Song Y. (2016). Fabrication of Bendable Circuits on a Polydimethylsiloxane (PDMS) Surface by Inkjet Printing Semi-Wrapped Structures. *Materials*, 9(4), 253.

- [2] FormFactor (2018). Cascade MPS150 150mm Manual Probe Station. [Datasheet]. <https://www.formfactor.com/download/mps150-data-sheet/?wpdmdl=3221&refresh=5df8036de34ba1576534893> (accessed on Aug. 2020).
- [3] Chen, S.P., Chiu, H.L., Wang, P.H., Liao, Y.C., (2015). Inkjet Printed Conductive Tracks for Printed Electronics. *ECS Journal of Solid State Science and Technology*, 4(4), 3026–3033.
- [4] Souk J., Morozumi S., Luo F.C., Bita I., (eds.). (2018). *Flat Panel Display Manufacturing*. John Wiley & Sons.
- [5] Yin, Z., Huang, Y., Bu, N., Wang, X., Xiong, Y. (2010). Inkjet printing for flexible electronics: Materials, processes and equipments. *Chinese Science Bulletin*, 55(30), 3383–3407.
- [6] Murty, Y.V. (2001). Electrical and electronic connectors: materials and technology. In Buschow, K.H.J., Cahn, R.W., Flemings, M.C., Ilshner, B., Kramer, E.J. *Encyclopedia of Materials: Science and Technology*. 2483–2494. Elsevier.
- [7] Fernandez-Pacheco, A. (2011). *Studies of Nanoconstrictions, Nanowires and Fe<sub>3</sub>O<sub>4</sub> Thin Films Electrical Conduction and Magnetic Properties. Fabrication by Focused Electron/Ion Beam*. Berlin Heidelberg: Springer Verlag.
- [8] Neff, C. (2018). *Analysis of Printed Electronic Adhesion, Electrical, Mechanical, and Thermal Performance for Resilient Hybrid Electronics*. [Doctoral Dissertation, University of South Florida]. <https://scholarcommons.usf.edu/etd/7551/> (accessed on Aug. 2020).
- [9] Mroczka, J. (2013). The cognitive process in metrology. *Measurement*, 46(8), 2896–2907.
- [10] Kamyshny, A., Magdassi, S. (2017). *Nanomaterials for 2D and 3D Printing*. Weinheim: Wiley-VCH.
- [11] Kang, J.S., Ryu, J., Kim, H.S., Hahn, H.T. (2011). Sintering of inkjet-printed silver nanoparticles at room temperature using intense pulsed light. *Journal of Electronic Materials*, 40, 2268.
- [12] Kim, D., Jeong, S., Moon, J., Kang, K. (2006). Ink-jet printing of silver conductive tracks on flexible substrates. *Molecular Crystals and Liquid Crystals*, 459(1), 45–55.
- [13] Caniggia, S., Maradei, S. (2008). *Signal Integrity and Radiated Emission of High-Speed Digital Systems, Appendix A: Formulae for Partial Inductance Calculation*. 481–486. Singapore: John Wiley & Sons, Ltd.
- [14] Aeffner, F., Hibret, A.A., Boyle, M.C, Cardiff, R.D., Hagendorn, E., Hoenerhoff, M.J., Klopffleisch, R., Newbigging, S., Schaudien, D., Turner, O., Wilson, K. (2018). Digital Microscopy, Image Analysis, and Virtual Slide Repository. *ILAR Journal*, 59(1), 66–79.
- [15] Vernon-Parry, K.D. (2000). Scanning electron microscopy: an introduction. *III-Vs Review*, 13(4), 40–44.
- [16] Grouvers, F.W. (1946). *Inductance calculations*. New York: Van Nostrand.
- [17] Khoo S.W., Saravanan K., Tan C.S. (2016). A Review of Surface Deformation and Strain Measurement Using Two-Dimensional Digital Image Correlation. *Metrology and Measurement Systems*, 23(3), 461–480.
- [18] Krupka J., Kamiński P., Kozłowski R., Surma B., Dierlamm A., Kwestarz M. (2015). Dielectric properties of semi-insulating silicon at microwave frequencies. *Applied Physics Letters*, 107(8), 082105.
- [19] Li, Y.G., Lu, D., Wong, C.P. (2009). Conductive Nano-Inks. In *Electrical conductive adhesives with nanotechnologies*. 303–360. Springer Science & Business Media.
- [20] Borkowski, J. (2012). Systematic errors of the LIDFT method: Analytical form and verification by a Monte Carlo method. *Metrology and Measurement Systems*, 19(4), 673–684.
- [21] Borkowski, J., Matuszewski, B.J., Mroczka, J., Shark, L.K. (2002). Geometric matching of circular features by least squares fitting. *Pattern Recognition Letters*, 23(7), 885–894.

- [22] Keithley. 2100 Series: 6½-Digit USB Multimeter. [Datasheet]. <https://www.tek.com/tektronix-and-keithley-digital-multimeter/keithley-2100-series-6%C2%BD-digit-usb-multimeter> (accessed on Aug. 2020).
- [23] Geyer, R.G. (1990). Dielectric Characterization and Reference Materials. *National Institute of Standards and Technology, Technical Note 1338*. U.S. Government Printing Office, Washington.
- [24] Kwiatkowski, P., Rózyc, K., Sawicki, M., Jachna, Z., Szplet, R. (2017). 5 ps jitter programmable time interval/frequency generator. *Metrology and Measurement Systems*, 24(1), 57–68.